J. COMBIN. MATH. COMBIN. COMPUT. 127a (2025) 5967--5991

Journal of Combinatorial Mathematics and Combinatorial Computing
www.combinatorialpress.com/jcmcc

# Optimization design of double gyro-swing reduction device in complex sea state based on nonlinear dynamic equations

Xinyu Gong[1,✉], Siqi Mao[2], Shixian Wu[1]

[1] *Faculty of Shipping and Ship Engineering, Chongqing Jiaotong University, Chongqing, 400074, China*

[2] *Hohai College, Chongqing Jiaotong University, Chongqing, 400074, China*

ABSTRACT

In order to enable ships to operate stably for a long time under complex sea conditions, all kinds of ships have an urgent need for gyroscopic rocking reduction devices. This paper takes the double gyro rocking reduction device with better rocking reduction effect as the research object, establishes its corresponding nonlinear dynamic equations, adopts the energy method to establish the differential equations of motion, and deduces the dynamic model of the rocking reduction double gyro. A parameter optimization model is established with the main objective of improving the shaking reduction effect, and the key components of the shaking reduction double gyro are optimized. The bacterial foraging optimization algorithm is selected to solve the model, and the multi-objective parameter optimization model is established. For one to five wave classes, the middle value of the wave height of the meaningful wave is selected for the dynamic simulation experiment of the double gyro. When the wave level is less than three time level, the rocking reduction performance of the rocking reduction double gyro reaches 87.5%, 78.1% and 77.78%, respectively, and the transverse rocking reduction performance is good. Under the simulation environment of sea state I (wave height 2.5m, average period 7s) and sea state II (righteous wave height 2.5m, average period 12s), the rocking reduction efficiencies of the ship after parameter optimization are improved by 6.44% and 10.09%, respectively.

*Keywords:* rocking reduction double gyro, nonlinear dynamic equation, parameter optimization, bacterial foraging optimization algorithm, multi-objective optimization model

## 1. Introduction

Complex sea conditions such as wind and waves, cloud cover, night travel, distribution of temperature, salinity and density, distribution of water masses and ocean circulation have caused non-negligible impacts on ship navigation. In the process of ship traveling, due to the driving of waves under the effect

✉ Corresponding author.
*E-mail address:* gongxinyu5925@163.com (X. Gong).
Received 25 February 2024; Revised 05 April 2024; Accepted 15 December 2024; Published Online 15 April 2025.
DOI: 10.61091/jcmcc127a-329

of wind, the ship will constantly sway, causing inconvenience to passengers and cargo. The emergence of the rocking gyro is to solve this problem.

Shake reduction gyro (ARG) is a common automatic stabilization device, using the principle of gyroscope to achieve, it is widely used in aircraft [1], ships [2], missiles [3], camera photography [4], medical [5], industrial processing [6] and other fields. And gyroscope is a device that utilizes the gyroscopic effect for measuring and controlling angular velocity [7]. The gyroscopic effect is when a gyroscopic body is subjected to external forces, its axis of rotation will change, which is due to the rotation of the gyroscopic body produces a moment, so that its axis of rotation deviation results [8]. The specific steps of the working principle of the swaying gyro are that the gyro body starts to rotate, generating a spin axis. When the ship shaking, shaking gyro will sense this shaking, and produce a moment in the opposite direction, the moment will make the gyro body rotational axis deviation, and produce a reaction force, so that the ship produces a shaking and shaking the opposite of the force, in the constant adjustment of the size and direction of the reaction force, the shaking gyro to achieve the ship to maintain a smooth, reduce shaking [9-10]. Reduced rocking gyro is not affected by the speed, sailing, mooring state can be reduced rocking; good suitability, cabin, deck, center, offset can be installed; no outstretched hull accessories, work does not affect the speed. Allow the installation of more than one, joint work, adapt to a larger ship [11-14]. Therefore, the gyro has now become the standard equipment for pilot boats, marine patrol boats and other boats.

In the optimization research of double gyro rocking reduction device, this paper firstly starts from the nonlinear dynamic equations of the rocking reduction double gyro device, puts forward the physical model of the rocking reduction double gyro device, and establishes its differential equations of motion from the kinetic energy of the ship's rocking, the kinetic energy of the rocking reduction gyro, and other aspects through the energy method. According to the momentum moment theorem, a single-frame control moment gyro dynamics model is established to obtain the dynamics equations of the sway-reducing double gyro in ship coordinates, and the turntable sway-reducing gyro is re-modeled by coordinate transformation. The transverse rocking angle of the ship is calculated with the help of the fourth-order Longecourt method, and the relevant objective functions of the rocking reduction effect, rotor mass and power drive are proposed. According to the size of the installation space inside the ship's cabin, the size constraints of the gyro rotor are given, and a multi-objective optimization model of the gyro rotor is established. The bacterial foraging optimization algorithm is selected from a variety of modern optimization algorithms, through which the multi-objective parameter optimization model of the ship's rocking reduction gyro is solved. Based on two measures of wave period and wave amplitude, we carry out the dynamic simulation experiments of double gyro under the environment of one to five level waves to test the effectiveness of the proposed double gyro device model. The "Jinghai" JH-750 unmanned boat of Shanghai University of China is used as an example to verify the accuracy of the proposed multi-objective optimization based rocking reduction double gyro parameter optimization model, and to carry out the rocking reduction double gyro parameter optimization simulation experiments.

## 2. Deconstrained double gyro model based on nonlinear dynamical equations

Ships require a rocking reduction system to resist wind and waves during navigation, thus enabling them to operate in a stable manner and improving safety and crew comfort. As a very effective rocking reduction device, the double gyro rocking reduction device has the advantage that it works entirely within the ship's hull and does not require sufficient movable mass to generate control moments. In this paper, based on the nonlinear dynamics equations, a dual gyro dynamics model for ship rocking reduction in complex sea conditions is established.

### *2.1. Nonlinear Dynamics Equations for a Double Gyroscopic Shake Reduction Device*

2.1.1. Movement of ships under wave action. A ship floating on water has six degrees of freedom of motion. If a coordinate system is established with the ship's bow and stern directions as $x$ axis, port and starboard directions as $y$ axes, and up and down directions as $z$ axes, then the translational movements along the $x,y,z$ directions are called longitudinal swing, transverse swing, and lifting and sinking, respectively; and the rotations around the $x,y$ and $z$ axes are called transverse rocking, longitudinal rocking, and ship rocking, respectively.

Since the shear capacity of water is extremely small, the ship floating on the water always inevitably under the action of non-zero external forces, including the motion of translation and rotation.

For displacement ships, the transverse rocking motion tends to be more violent because the moment of inertia of the transverse rocking motion is smaller. In other words, reducing the transverse rocking of ships is the main topic in the study of ship stabilization.

2.1.2. Physical modeling of the reduced-swing double gyro. A power gyro is used to stabilize a ship in waves according to the two following physical properties of the gyro.
1) The application of an external moment to a free gyro causes an angular displacement of the gyro in the plane formed by the external moment vector and the spin axis of the gyro rotor, which is usually referred to as the feed.
2) The gyro advance produces a gyroscopic moment proportional to the angular velocity of the gyro advance, acting in the plane formed by the advance axis and the spin axis of the gyro rotor. The moment appears in the form of the bearing reaction force of the feed shaft.

According to theoretical mechanics, the gyroscopic stabilizing moment can be written as the following equation:

$$M_a = j_a \omega_a \dot{\psi}_p \tag{1}$$

Where, $j_a$ is the rotational inertia of the gyro rotor relative to its own axis of gyration; $\omega_a$ is the gyro rotor's slewing speed; $\dot{\psi}_p$ is the gyro rotor's feed speed; $M_a$ is the external moment applied to the gyro.

Formula (1) for the theoretical basis of the role of gyro stabilization.

2.1.3. Equations of motion. The energy method is used to establish the differential equations of motion of the system, all physical quantities are in SI units and the energy terms of the system are as follows.
1) Kinetic energy of the ship's rocking:

$$T_1 = \frac{1}{2} I_1 \dot{\theta}^2 \tag{2}$$

where $I_1$ represents the moment of inertia of the ship, and since the moment of inertia of the ship is much larger than that of the deceleration gyro, the moment of inertia of the deceleration gyro can be ignored.
2) Kinetic energy of the deceleration gyro. Noting that the maximum gyro advance angle is usually not more than 30°, with the approximation $\sin\dot{\psi}_p \approx \dot{\psi}_p, \cos\dot{\psi}_p \approx 1$, it can be expressed as:

$$T_2 = \frac{1}{2} j_a (\omega_a + \dot{\theta}\psi_p)^2 + \frac{1}{2}(j_b + j_0)\dot{\psi}_p^2 \tag{3}$$

Where $j_b$ is the moment of inertia of the gyro relative to the frame axis; $j_0$ is the moment of inertia of the gyro frame relative to the frame axis.
3) The total kinetic energy of the ship-decoupled gyro system:

$$T=\frac{1}{2}I_1\dot{\theta}^2+\frac{1}{2}j_a\omega_a+\dot{\theta}\psi_p^2+\frac{1}{2}(j_b+j_0)\dot{\psi}_p^2 \tag{4}$$

Take the center of gravity of the frame and gyro system to lie below the trunnion of the frame.

4) Potential energy of the system:

$$U=\frac{1}{2}H_c\psi_p^2+\frac{1}{2}Dh\theta^2 \tag{5}$$

Where, $H_c$ is the static moment of the decoupled gyro.

5) Dissipated energy of the system from friction between the ship and the water and air:

$$\Phi=N_\theta\dot{\theta}^2 \tag{6}$$

The dissipated energy from friction on the trunnions of the gyro frame is omitted. Denote the wave disturbance moment by $Dh_\theta\varphi\gamma_s\sin\omega t$, where $D$ is the displacement of the ship, $h\theta$ is the initial stability height of the ship, $\gamma_e$ is the effective wave inclination angle of the wave, and $\sin\omega t$ denotes the variation of a harmonic wave of frequency $\omega$ with time $t$.

On the active decoupling gyro, it is assumed that what causes the realization of the gyro driving action is the simple harmonic moment that causes the inlet, and the action itself is quasi-elastic, that is, it is allowed that there is a phase difference between the oscillation of the gyro frame and the action, which is equivalent to a periodic action pay $A_a\cos(\omega t+\varepsilon)$ affecting the inlet in terms of the equations of motion.

Then the differential equations of motion of the ship a gyro system are obtained from Eq. (2) to Eq. (6):

$$\begin{cases}(I_1+j_a\psi^2)\ddot{\theta}+N_\theta\dot{\theta}+Dh\theta+J_a\omega_a\dot{\psi}_p=Dh\gamma_a\sin\omega\\(j_b+j_0)\ddot{\psi}+H_c\psi_P-J_a\omega_a\dot{\theta}=A_a\cos(\omega t+\varepsilon)\end{cases} \tag{7}$$

Since $j_a\psi^2$ is much less than $I_1$, it can be ignored. Let:

$$2v=N_\theta/I_1;n^2=Dh/I_1;\alpha_g=j_a\omega_a/I_1$$
$$m_p^2=\frac{H_c}{j_b+j_0};c_j=\frac{I_1}{j_b+j_0};a_a=\frac{A_a}{j_b+j_0} \tag{8}$$

The system of equations (7) can be rewritten as:

$$\begin{cases}\ddot{\theta}+2v\dot{\theta}+n^2\theta+\alpha_g\dot{\psi}_p=n^2\gamma_e\sin\omega t\\\ddot{\psi}+m_p^2\psi_P-\alpha_g c_j\dot{\theta}=a_a\cos(\omega t+\varepsilon)\end{cases} \tag{9}$$

### 2.2. Ship Deceleration Double Gyro Dynamic Modeling

2.2.1. Single-frame control moment gyro dynamics modeling. The deceleration gyro is mounted on the hull deck, and consists of an outer frame, a feed shaft, a rotor, and a rotor spin axis. $o\xi\eta\zeta$ is the ground coordinate system with the center of the earth as the origin, where $O\zeta$ is perpendicular to the ground, and $\phi$ is the transverse rocking angle of the hull around the axis $O\zeta$. $Oxyz$ is the gyro coordinate system with the center of gravity of the gyro as the origin, the center of gravity of the gyro coincides with the center of the earth, $Oy$ axis for the gyro's axis of advancement, $Oz$ for the rotor's axis of rotation, and $\beta$ for the gyro's angle of advancement around $Oy$ axis.

Assume that the angular velocity of rotation of the ship is projected on the base coordinate system $O-\xi\eta\zeta$:

$$\Omega=\left[\Omega_\xi,\Omega_\eta,\Omega_\zeta\right] \tag{10}$$

Since the frame coordinate system $O-xyz$ does not affect the rotation of the gyro rotor, it can be obtained by considering $O-xyz$ as a projected coordinate system and then projecting the base angular velocity $\Omega$ from Eq. (10) onto $O-xyz$:

$$\begin{cases} \Omega_x = \Omega_\xi \cos\beta - \Omega_\zeta \sin\beta \\ \Omega_y = \Omega_\eta \\ \Omega_z = \Omega_\xi \sin\beta + \Omega_\zeta \cos\beta \end{cases} \tag{11}$$

Since the gyro has a feed in the $O_y$-axis, the angular velocity of the feed is added to the ship's coordinate system $O-xyz$, which can be obtained by decomposing the angular velocity into the $O-xyz$-coordinate:

$$\omega = \left[\omega_x, \omega_y, \omega_z\right] = \left[\Omega_x, \dot{\beta} + \Omega_y, \Omega_z\right] \tag{12}$$

Assume that the moments of inertia of the gyro rotor in the three axes of coordinate system $O-x_R y_R z_R$ are $A_R, B_R, C_R$, and the moments of inertia of the gyro frame in the three axes of gyro coordinate system $O-xyz$ are $A, B, C$. Then the combined moments of force exerted on the gyro rotor and the gyro frame are projected onto the coordinate system $O-xyz$, and let the projected moment be $M$, and the projection of the moment of momentum $H_R$ generated by the point $O$ in the gyro rotor into the coordinate system $O-xyz$ is [15]:

$$H_R = \left[A_R\omega_x, B_R\omega_y, C_R(\omega_z + \dot{\phi})\right] \tag{13}$$

The projection of the momentum moment $H_0$ generated by the frame to the point $O$ within the coordinate system $O-xyz$ can be expressed as:

$$H_0 = \left[A\omega_x, B\omega_y, C\omega_z\right] \tag{14}$$

Then the total momentum moment $H$ generated by the gyro frame and gyro rotor for point $O$ is:

$$H = H_R + H_0 = \left[(A_R + A)\omega_x, (B_R + B)\omega_y, C_R(\omega_z + \dot{\phi}) + C\omega_z\right] \tag{15}$$

According to the Moment of Momentum Theorem, there are in coordinate system $O-xyz$:

$$\frac{dH}{dt} + \omega \times H = M \tag{16}$$

And so it can be obtained:

$$\begin{cases} M_x = (A_R + A)\dot{\omega}_x - (B_R + B)\omega_y\omega_z + (C_R(\omega_z + \dot{\phi}) + C\omega_z)\omega_y \\ M_y = (B_R + B)\dot{\omega}_y + (A_R + A)\omega_x\omega_z - (C_R(\omega_z + \dot{\phi}) + C\omega_z)\omega_x \\ M_z = \dfrac{d(C_R(\omega_z + \dot{\phi}) + C\omega_z)}{dt} + (B_R + B)\omega_y\omega_x - (A_R + A)\omega_x\omega_y \end{cases} \tag{17}$$

Let the rotating momentum moment constant be $h_0 = C_R\omega_0$ and let the steady state value of rotor speed be $\omega_0 = \omega_z + \dot{\phi}$. Equation (18) can be further calculated as:

$$\begin{cases} M_x = A_R\dot{\Omega}_\xi \cos\beta - A_R\dot{\Omega}_\zeta \sin\beta + h_0\dot{\beta} - 2\dot{\beta}A_R(\Omega_\xi \sin\beta + \Omega_\zeta \cos\beta) \\ -\Omega_\eta(A_R\Omega_\xi \sin\beta + A_R\Omega_\zeta \cos\beta - h_0) \\ M_y = A_R\ddot{\beta} + A_R\dot{\Omega}_\eta + A_R(\Omega_\xi^2 - \Omega_\zeta^2)\sin\beta\cos\beta + A_R\Omega_\xi\Omega_\xi(\cos^2\beta - \sin^2\beta) \\ -h_0(\Omega_\xi \cos\beta - \Omega_\zeta \sin\beta) \\ M_z = 0 \end{cases} \tag{18}$$

It is now assumed that the base follows the angular velocity $\Omega=[\Omega_\zeta,\Omega_\eta,\Omega_\xi]=[\dot{\phi},\dot{\theta},\dot{\upsilon}]$ of the $O$-point sway, where $\dot{\phi},\dot{\theta},\dot{\upsilon}$ represents the angular velocities of transverse, longitudinal, and bow sway, respectively.

The value of the rotational momentum moment constant $h_0$ in Eq. (18) is much larger compared to the ship's angle of rotation, angular velocity and moment of inertia. Therefore, in order to further simplify the model, the higher order terms in Eq. (18) can be ignored, and at the same time, the coupling between the ship's transverse rocking and the states of motion in the other five degrees of freedom can be ignored into the rotational momentum moment constant $J = A_R$, and then the dynamical equations of the gyro in the ship's coordinates $O-xyz$ can be expressed as:

$$\begin{cases} M_x = h_0\dot{\beta} \\ M_y = J\ddot{\beta} - h_0\dot{\phi}\cos\beta \\ M_z = 0 \end{cases} \tag{19}$$

The projection of Eq. (19) into the base coordinate system $O-\xi\eta\zeta$ can be obtained:

$$\begin{cases} M_\xi = h_0\dot{\beta}\cos\beta \\ M_\eta = J\ddot{\beta} - h_0\dot{\phi}\cos\beta \\ M_\zeta = h_0\dot{\beta}\sin\beta \end{cases} \tag{20}$$

2.2.2. Dynamic modeling of a rotating-disk decoupling gyro. Compared with the conventional swing-reducing gyro, the rotor of the turntable-type swing-reducing gyro is placed vertically instead of horizontally, and then its dynamics model is different from that of the conventional swing-reducing gyro, which needs to be re-established.

The frame inlet axis, which is parallel to the ground, is changed to be perpendicular to the ground, and the rotor axis, which is perpendicular to the ground, is changed to be half-way to the ground, i.e., the frame inlet axis and the rotor axis are exchanged in different directions. The three axes of the gyro are the torque output axis, the frame feed axis and the rotor spin axis, which are perpendicular to each other. In contrast, the rotor-type deceleration gyro only exchanges the direction of the rotor spin axis and the frame inlet axis, and does not affect the torque output axis. Therefore, the dynamics model is re-established as follows:

$$\begin{cases} M_\xi = h_0\dot{\beta}\cos\beta \\ M_\eta = h_0\dot{\beta}\sin\beta \\ M_\zeta = J\ddot{\beta} - h_0\dot{\phi}\cos\beta \end{cases} \tag{21}$$

In order to provide a higher damping torque, multiple dampers are placed in the inlet direction of the turntable type damping gyro. The telescopic movement of the damper rod results in unequal hydraulic oil pressures in the two chambers of the damper rod, creating a pressure differential, and the side with the higher oil pressure presses the fluid bush oil towards the damping hole, and thus the damping moment provided for the feed of the frame shaft of the rocking reduction gyro is created.

Assume that the damping moment is:

$$M_{zn} = C\dot{\beta} \tag{22}$$

Where: $C$ represents the damping coefficient, the specific value of which is determined according to different models of dampers with the diameter of the small holes on the corresponding dampers.

Adding the damping moment to Eq. (21), then the dynamics model of the rotating disk type rocking reduction gyro can be expressed as:

$$\begin{cases} M_{\xi} = h_0\dot{\beta}\cos\beta \\ M_{\eta} = h_0\dot{\beta}\sin\beta \\ M_{\zeta} = J\ddot{\beta} - h_0\dot{\phi}\cos\beta + C\dot{\beta} \end{cases} \tag{23}$$

## 3. Optimization model of shaking-reducing dual gyro parameters based on multi-objective optimization

This chapter will optimize the parameters of key components such as rotor and inlet damper of the sway-reducing double gyro device to further improve the sway-reducing effect. Optimization of key components parameters means that the optimized ship rocking reduction gyro has higher space utilization, lower energy consumption, less material consumption, lower cost, and its corresponding rocking reduction effect is higher.

### *3.1. Calculation of ship's transverse rocking angle*

First solve for the ship's transverse rocking angle $\phi_N$ when the deceleration gyro is not working. order $x = \phi_N'$, the time range is $t \in [a,b]$, and define the transverse rocking angle and transverse rocking angular velocity initial value is zero, which can be defined $\phi_N(a) = 0, \phi_N'(a) = x(a) = 0$, which is then transformed into a system of first-order differential equations initial value problem:

$$\begin{cases} \phi_{N'}(t) = x(t) & t \in [a,b] \\ x'(t) = f(t, \phi_N(t), x(t)), & t \in [a,b] \\ x(a) = \phi_{N'}(a) = 0, \phi_N(a) = 0 \end{cases} \tag{24}$$

In the formula:

$$\begin{aligned} f(t, \phi_N(t), x(t)) = -c_1 x(t) - c_3 x(t)^3 - k_1\phi_N(t) - k_3\phi_N(t)^3 \\ -k_5\phi_N(t)^5 + Dh\alpha(t)/(I_{\phi\phi} + J_{\phi\phi}) \end{aligned} \tag{25}$$

In turn, solving the above initial value problem for a system of first order differential equations using the fourth order Lungkuta method leads to the following numerical form [16]:

$$\begin{cases} \phi_{N(k+1)} = \phi_{Nk} + \dfrac{h}{6}(K_1 + 2K_2 + 2K_3 + K_4) \\ x_{k+1} = x_k + \dfrac{h}{6}(L_1 + 2L_2 + 2L_3 + L_4) \end{cases} \tag{26}$$

where $h$ is the iteration step at time $t$, $k$ is the number of iterations, and $K_1, K_2, K_3, K_4, L_1, L_2, L_3, L_4$ is the coefficient of the Lungkuta method of solving and can be expressed as:

$$\begin{cases} K_1 = x_k, L_1 = f(t_k, \phi_{Nk}, x_k) \\ K_2 = x_k + \frac{h}{2}L_1, L_2 = f(t_k + \frac{h}{2}, \phi_{Nk} + \frac{h}{2}K_1, x_k + \frac{h}{2}L_1) \\ K_3 = x_k + \frac{h}{2}L_2, L_3 = f(t_k + \frac{h}{2}, \phi_{Nk} + \frac{h}{2}K_2, x_k + \frac{h}{2}L_2) \\ K_4 = x_k + \frac{h}{2}L_3, L_4 = f(t_k + \frac{h}{2}, \phi_{Nk} + \frac{h}{2}K_3, x_k + \frac{h}{2}L_3) \end{cases} \tag{27}$$

In turn, it is possible to obtain a numerical expression for the change in the transverse rocking angle $\phi_N$ following the time $t$ when the decelerating gyro is not in operation:

$$\phi_{N(k+1)} = \phi_{Nk} + \frac{h}{6}(K_1 + 2K_2 + 2K_3 + K_4) \tag{28}$$

Since the above equation is a numerical solution, i.e., a collection of discrete points, scholars usually solve the standard deviation of the values of the discrete points of the transverse rocking angle as the evaluation standard of the ship's transverse rocking angle on the time period $t \in [a,b]$, then the standard deviation of the transverse rocking angle $\phi_N$ can be obtained when the decelerating gyroscope is not working $S(\phi_N)$ is:

$$S(\phi_N) = \sqrt{\frac{\sum_{i=1}^{k}(\phi_{Ni} - \overline{\phi}_N)^2}{k-1}} \tag{29}$$

Where $k$ is the number of iterations in solving the numerical solution process, $i \in k$, $\overline{\phi}_N$ is the average value of the ship's transverse rocking angle at each discrete point on the time period $t \in [a,b]$.

Then solve the deceleration gyro work, the ship transverse rocking angle $\phi_o$. Order $x = \phi_0', y = \beta'$, the time range is $t \in [a,b]$, and define the transverse rocking angle and transverse rocking angular velocity, into the angle and into the initial value of angular velocity of zero, that is, $\phi_N(a) = 0, \phi_N'(a) = x(a) = 0, \beta(a) = 0, \beta'(a) = y(a) = 0$, then can be transformed into a system of first-order differential equations of the first-order value of the problem:

$$\begin{cases} \phi_O'(t) = x(t) & \mathrm{t} \in [a,b] \\ \beta'(t) = y(t) & \mathrm{t} \in [a,b] \\ x'(t) = f_1(t, \phi_O(t), x(t), \beta(t), y(t)) & \mathrm{t} \in [a,b] \\ y'(t) = f_2(t, x(t), \beta(t), y(t)) & \mathrm{t} \in [a,b] \\ x(a) = \phi_O'(a) = 0, \phi_O(a) = 0 \\ y(a) = \beta'(a) = 0, \beta(a) = 0 \end{cases} \tag{30}$$

In the formula:

$$\begin{cases} f_1(t, \phi_O(t), x(t), \beta(t), y(t)) = -c_1 x(t) - c_3 x(t)^3 - k_1 \phi_O(t) - k_3 \phi_O(t)^3 - k_3 \phi_O(t)^5 \\ -2h_0 y(t) \cos\beta(t) / (I_{\phi\phi} + J_{\phi\phi}) + Dh\alpha(t) / (I_{\phi\phi} + J_{\phi\phi}) \\ f_2(t, x(t), \beta(t), y(t)) = h_0 x(t) \cos\beta(t) / J - my(t) / J \end{cases} \tag{31}$$

In turn, solving the above initial value problem for the system of first order differential equations using the fourth order Lungkuta method leads to the following numerical form:

$$\begin{cases} \phi_{O(k+1)} = \phi_{Ok} + \dfrac{h}{6}(K_{11} + 2K_{12} + 2K_{13} + K_{14}) \\ x_{k+1} = x_k + \dfrac{h}{6}(L_{11} + 2L_{12} + 2L_{13} + L_{14}) \\ \beta_k = \beta_k + \dfrac{h}{6}(K_{21} + 2K_{22} + 2K_{23} + K_{24}) \\ y_{k+1} = y_k + \dfrac{h}{6}(L_{21} + 2L_{22} + 2L_{23} + L_{24}) \end{cases} \tag{32}$$

where: $h$ is the iteration step at time $t$ , $k$ is the number of iterations, $K_1 1, K_{12}, K_{13}, K_{14}, K_{21}, K_{22}, K_{23}, K_{24}$, $L_{11}, L_{12}, L_{13}, L_{14}, L_{21}, L_{22}, L_{23}, L_{24}$ are the coefficients of the Lungkuta method of solving and can be written as:

$$\begin{cases} K_{11} = x_k, L_{11} = f_1(t_k, \phi_{Ok}, x_k, \beta_k, y_k) \\ K_{12} = x_k + \dfrac{h}{2}L_{11}, L_{12} = f_1\left(t_k + \dfrac{h}{2}, \phi_{0k} + \dfrac{h}{2}K_{11}, x_k + \dfrac{h}{2}L_{11}.\beta_k + \dfrac{h}{2}K_{21}, y_k + \dfrac{h}{2}L_{21}\right) \\ K_{13} = x_k + \dfrac{h}{2}L_{12}, L_{13} = f_1\left(t_k + \dfrac{h}{2}, \phi_{Ok} + \dfrac{h}{2}K_{12}, x_k + \dfrac{h}{2}L_{12}, \beta_k + \dfrac{h}{2}K_{22}, y_k + \dfrac{h}{2}L_{21}\right) \\ K_{14} = x_k + \dfrac{h}{2}L_{13}, L_{14} = f_1\left(t_k + \dfrac{h}{2}, \phi_{0k} + \dfrac{h}{2}K_{13}, x_k + \dfrac{h}{2}L_{13}, \beta_k + \dfrac{h}{2}K_{23}, y_k + \dfrac{h}{2}L_{21}\right) \\ K_{21} = y_k, L_{21} = f_2(t_k, x_k, \beta_k, y_k) \\ K_{22} = y_k + \dfrac{h}{2}L_{21}, L_{22} = f_2\left(t_k + \dfrac{h}{2}, x_k + \dfrac{h}{2}L_{11}.\beta_k + \dfrac{h}{2}K_{21}, y_k + \dfrac{h}{2}L_{21}\right) \\ K_{23} = y_k + \dfrac{h}{2}L_{22}, L_{23} = f_2\left(t_k + \dfrac{h}{2}, x_k + \dfrac{h}{2}L_{12}, \beta_k + \dfrac{h}{2}K_{22}, y_k + \dfrac{h}{2}L_{21}\right) \\ K_{24} = y_k + \dfrac{h}{2}L_{23}, L_{24} = f_2\left(t_k + \dfrac{h}{2}, x_k + \dfrac{h}{2}L_{13}, \beta_k + \dfrac{h}{2}K_{23}, y_k + \dfrac{h}{2}L_{21}\right) \end{cases} \tag{33}$$

In turn, it is possible to obtain a numerical expression for the change of the transverse rocking angle $\phi_O$ with time $t$ during the operation of a decelerating gyro:

$$\phi_{O(k+1)} = \phi_{Ok} + \frac{h}{6}(K_1 + 2K_2 + 2K_3 + K_4) \tag{34}$$

Since the above equation is a numerical solution, i.e., a collection of discrete points, scholars usually solve the standard deviation of the values of the discrete points of the transverse rocking angle as the evaluation standard of the transverse rocking angle of the ship on the time period $t \in [a,b]$, then the standard deviation of the transverse rocking angle $\phi_O$ during the work of the decelerating gyro can be obtained $S(\phi_O)$ is:

$$S(\phi_O) = \sqrt{\frac{\sum_{i=1}^{k}(\phi_{Oi} - \overline{\phi}_O)^2}{k-1}} \tag{35}$$

where $k$ is the number of iterations in the process of solving the numerical solution, $i \in k$, $\overline{\phi}_O$ are the average values of the ship's transverse rocking angle at each discrete point on time period $t \in [a,b]$.

### 3.2. *Objective function*

1) Optimization of the effect of rocking reduction. The current standard for judging the effectiveness

of the ship's rocking reduction gyro is the size of the rocking reduction rate, which is defined as $s$:

$$S = \frac{S(\phi_N) - S(\phi_O)}{S(\phi_N)} \times 100\% \tag{36}$$

Then the optimization objective of the shake reduction effect is:

$$\min f_1(D_1, D_2, D_3, H_1, H_2, H_3, \omega, m) = 1 - S \tag{37}$$

2) Optimization of rotor mass. In the optimization design will involve lightweight design, that is, to reduce the weight of the product, in order to reduce the cost at the same time to facilitate the installation. In the overall components of the ship decoupling gyro, the main mass is concentrated in the gyro rotor, and the mass of the gyro rotor can be expressed as:

$$M = \rho V = \rho(H_1(D_2 - D_1) + 2H_3D_1 + H_2D_3) \tag{38}$$

Then the goal of lightweighting the ship's rocking reduction gyro is:

$$\begin{aligned} &\min f_2(D_1, D_2, D_3, H_1, H_2, H_3, \omega, m) \\ &= \rho(H_1(D_2 - D_1) + 2H_3D_1 + H_2D_3) \end{aligned} \tag{39}$$

3) Optimization of power drive. Considering the finite nature of the supplyable power of the ship's power system, the design of the motor drive needs to consider the driving torque of the motor as well as the rotational speed, the most important of which is the motor speed also as the rotor speed. A suitable motor speed can avoid excessive consumption of energy from the ship's power system, and the speed of the motor is $\omega$ .

Then the objective of ship power drive optimization is:

$$\min f_3(D_1, D_2, D_3, H_1, H_2, H_3, \omega, m) = \omega \tag{40}$$

### *3.3. Constraints*

According to the size of the installation space inside the ship's cabin, the dimensional constraints of the gyro rotor are given. Assuming that the size of the installable space in the ship's cabin is $h_l \times h_w \times h_h$, the following constraints should be satisfied for the gyro rotor OD $D_1$, rotor ID $D_2$, rotor diameter $D_3$, rotor wall thickness $H_1$, rotor length $H_2$, and rib plate thickness $H_3$:

$$\begin{cases} D_2 < D_1 < \min(h_l, h_w, h_h) \\ a_1 < D_2 \\ a_2 < D_3 < a_3 \\ H_1 < H_2 < \min(h_l, h_w, h_h) \\ a_4 < H_1 \\ a_5 < H_3 < a_6 \end{cases} \tag{41}$$

Where: $a_i, i \in (1,6)$ are positive numbers, and the specific values are based on the actual situation.

According to the supplyable power of the ship's power system, the constraints on the motor speed are given; assuming that the supplyable power is $P_b$, due to $\omega = \frac{9550P}{T}$, where $P$ is the rated power and $T$ is the rated torque, the motor speed needs to satisfy the following constraints:

$$a_7 < \omega \le \frac{9550P_b}{T} \tag{42}$$

The constraints can be summarized as follows:

$$s.t.\begin{cases} D_2 < D_1 < \min(h_l, h_w, h_h), a_1 < D_2 \\ H_1 < H_2 < \min(h_l, h_w, h_h), a_4 < H_1 \\ a_2 < D_3 < a_3, a_5 < H_3 < a_6, a_7 < \omega \le \dfrac{9550P_b}{T} \\ a_8 \le m \le a_9, a_{10} \le S \le a_{11} \end{cases} \tag{43}$$

Where: $a_i, i \in (1,11)$ are positive numbers, the exact value depends on the actual situation.

### *3.4. Optimization model for the parameters of the decoupling gyro*

According to the actual situation of ship rocking gyro and ship, this paper establishes three objective functions, as shown in Equation (37), Equation (39) and Equation (40). These three objective functions have a relationship between the connection and mutual constraints. Then, considering these three objective functions, a multi-objective optimization model can be established to optimize the parameters of the key components of the ship's deceleration gyro:

$$\begin{cases} \begin{cases} \min f_1(D_1, D_2, D_3, H_1, H_2, H_3, \omega, m) = 1 - S \\ \min f_2(D_1, D_2, D_3, H_1, H_2, H_3, \omega, m) = \rho(H_1(D_2 - D_1) + 2H_3D_1 + H_2D_3) \\ \min f_3(D_1, D_2, D_3, H_1, H_2, H_3, \omega, m) = \omega \end{cases} \\ s.t.\begin{cases} D_2 < D_1 < \min(h_l, h_w, h_h), a_1 < D_2 \\ H_1 < H_2 < \min(h_l, h_w, h_h), a_4 < H_1 \\ a_2 < D_3 < a_3, a_5 < H_3 < a_6, a_7 < \omega \le \dfrac{9550P_b}{T} \\ a_8 \le m \le a_9, a_{10} \le S \le a_{11} \end{cases} \end{cases} \tag{44}$$

Where: $a_i, i \in (1,11)$ are positive numbers, the exact value depends on the actual situation.

### *3.5. Principles of Bacterial Foraging Optimization Algorithm*

Bacterial foraging behavior can be mainly summarized as: searching for food, moving position, digesting food, and mimicking such foraging behavior an intelligent algorithm is proposed as - Bacterial Foraging Optimization Algorithm, which mainly consists of three steps: chemotaxis, replication, and migration operations.

The main parameters of the bacterial foraging algorithm are as follows [17]. $N_p$ is the population size, $P_{ed}$ is the migration probability, $N_{ed}$ is the number of migration operations, $N_r$ is the number of replication operations, $N_\varepsilon$ is the maximum step size of unidirectional bacterial movement in the chemotaxis operation, and $N_c$ is the number of chemotaxis operations.

1) Chemotaxis operation. The chemotaxis operation is the key part of the bacterial foraging algorithm, chemotaxis is the behavior of bacteria swimming towards the nutrient-rich places and piling up, which has the advantage of finding the local optimal solution. The initialization of the bacterial foraging algorithm uses random initialization with the following formula:

$$X = X_{\min} + rand * (X_{\max} - X_{\min}) \tag{45}$$

Where: $X_{\min}$ and $X_{\max}$ are the minimum and maximum values in the optimization range, and $X$ is the initialized position of the bacteria.

In turn, the latest position of the bacteria after each chemotaxis operation can be expressed as:

$$P(i, j+1, k, l) = P(i, j, k, l) + C(i) * \frac{\Delta(i)}{\sqrt{\Delta^T(i)\Delta(i)}} \tag{46}$$

where $P(i, j+1, k, l)$ and $P(i, j, k, l)$ denote the positions of bacteria $i$ after realizing the $j+1$th and $j$th chemotaxis operations under the $k$th replication operation and the $l$th migration operation, respectively. $C(i)$ is the chemotaxis step of bacteria $i$, and $\Delta(i)$ is the unit random direction vector. The initial value is set to $i=0$.

2) Replication operation. The replication operation accurately expresses the idea of Darwin's theory of evolution - the survival of the fittest: the bacteria with low survival ability will be discarded, and the remaining bacteria with relatively strong survival ability will be retained, and will continue to replicate to ensure that the size of the population remains unchanged.

3) Migration. The migration operation is to expand the area in which the bacteria feed to avoid clustering of bacteria together, and thus to avoid falling into a local optimum solution during the solution process. As long as the bacteria satisfy the migration condition, a randomly generated bacteria with probability less than the originally set probability of the migration operation, i.e., $rand() < P_{ed}$, then this bacteria dies out. Then a brand new bacterial individual is randomly generated at a certain location within the globe to ensure that the total number of populations remains unchanged. The initial value is set to $i=0$ and rand is a random value between [0, 1].

### 3.6. Multi-objective optimization model

First, the optimal solution $f_1^*(x,y,z)$ of each single-objective function is solved separately as the ideal point. Then, the evaluation function of each single-objective function is established for the straight line spacing between the actual point and the ideal point:

$$F_i\left(D_1,D_2,D_3,H_1,H_2,H_3,\omega,m\right)=\begin{bmatrix} f_i\left(D_1,D_2,D_3,H_1,H_2,H_3,\omega,m\right) \\ -f_i^*\left(D_1,D_2,D_3,H_1,H_2,H_3,\omega,m\right)\end{bmatrix}^2 \tag{47}$$

Finally, based on Eq. (47), the weight coefficients $\alpha_j$ are added and the sum of each weight coefficient is 1, which in turn transforms the expression (44) of multi-objective optimization into a multi-objective optimization model as:

$$\begin{aligned}&\min f\left(D_1,D_2,D_3,H_1,H_2,H_3,\omega,m\right)\\ &=\left\{\sum_{j=1}^{3}\alpha_j\cdot\begin{bmatrix} f_j\left(D_1,D_2,D_3,H_1,H_2,H_3,\omega,m\right) \\ -f_j^*\left(D_1,D_2,D_3,H_1,H_2,H_3,\omega,m\right)\end{bmatrix}^2\right\}^{\frac{1}{2}}\end{aligned} \tag{48}$$

$$s.t.\begin{cases} D_2 < D_1 < \min(h_l,h_w,h_h), a_1 < D_2 \\ H_1 < H_2 < \min(h_l,h_w,h_h), a_4 < H_1 \\ a_2 < D_3 < a_3, a_5 < H_3 < a_6, a_7 < \omega \le \dfrac{9550P_b}{T} \\ a_8 \le m \le a_9, a_{10} \le S \le a_{11}\end{cases} \tag{49}$$

Where $a_i, i\in(1,11)$ are positive numbers, the exact value depends on the actual situation.

## 4. Simulation experiments on the dynamics of a decoupled double gyro in complex sea states

In this chapter, we will use Adams to carry out a dynamics simulation experiment on the rocking-reducing dual gyroscope device model established in the previous section to verify its rocking-reducing performance and explore its rocking-reducing law.

The simulation experiment is based on two measures of wave period and wave amplitude. However, for different wave levels, the meaningful wave height of each wave level has a certain interval range, in order to make the simulation data more accurate, for any level of waves, the middle value of the meaningful wave height is selected for simulation.

### 4.1. *Analysis of the performance of primary wave attenuation*

The simulation results obtained by taking the middle value of wave height of 0.05 meters under the first level of sea state with sense wave are shown in Fig. 1. Figure (a)~Figure (c) for the ship's wave inclination angle, double gyro rotor speed of 0r/min and 6000r/min when the ship's transverse rocking angle simulation results output curve. From the graph, it can be concluded that at this time, the wave inclination angle of 0 to 4 degrees, the gyro rotor speed of 0r/min, the ship's transverse rocking angle of 0 to 3.2 degrees, the gyro rotor speed of 6000r/min, the ship's transverse rocking angle of the maximum near 0 to 0.4 degrees, the ability to reduce the rocking is 87.5%.

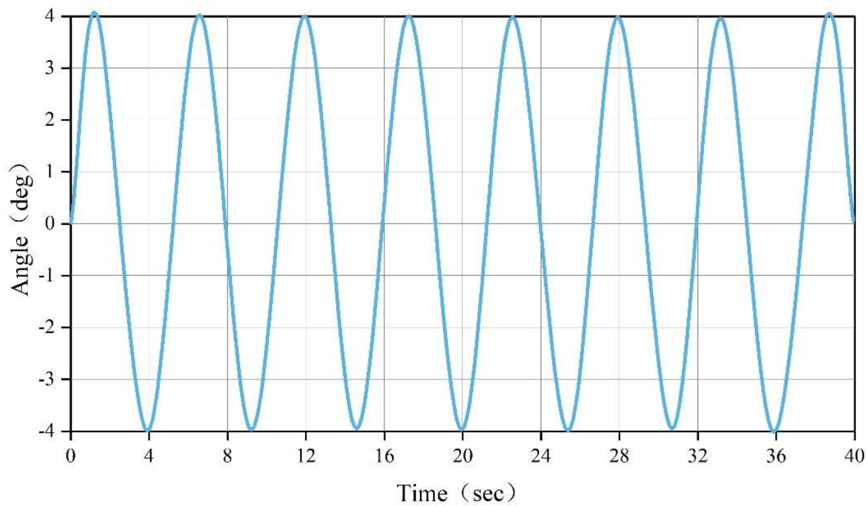


(a) Wave slope

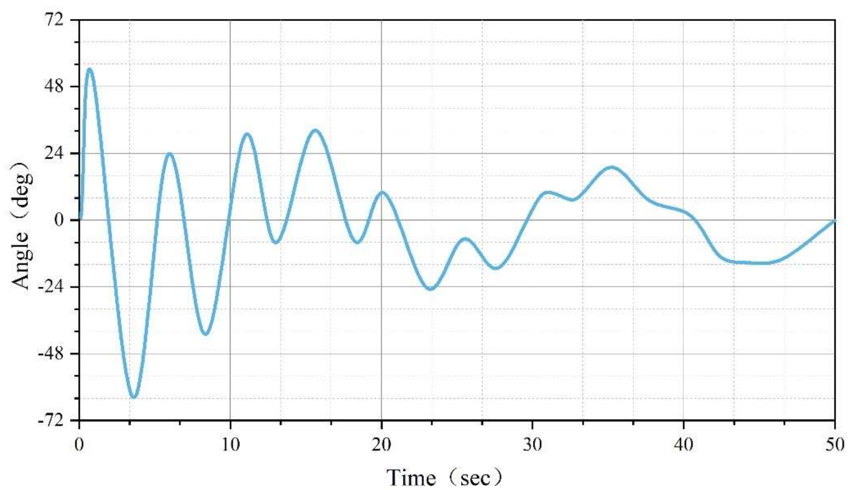


(b) The simulation results of 0r/min

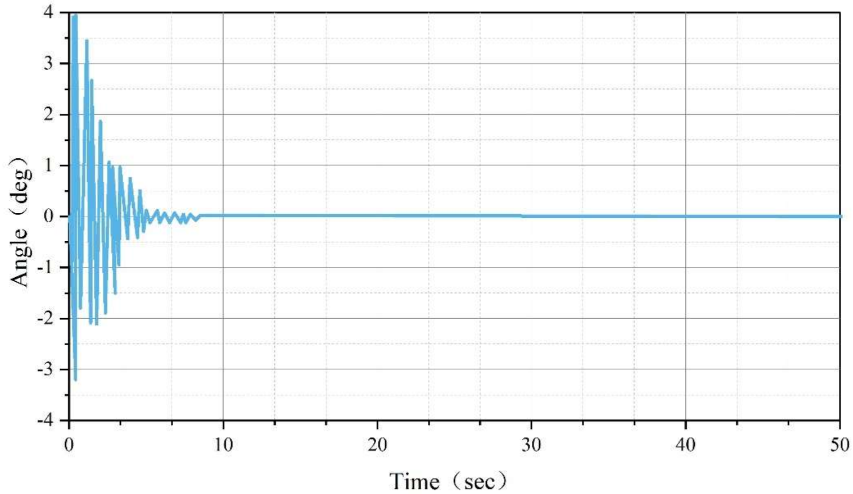


(c) The simulation results of 6000r/min

**Fig. 1.** The simulation results of first-order waves

### *4.2. Performance analysis of secondary wave attenuation*

Under the secondary waves, taking the middle value of wave height 0.25 m, the simulation results of the ship's transverse rocking are specifically shown in Fig. 2, and Figs. (a) to (c) show the ship's wave inclination angle, the ship's transverse rocking angle when the double gyro rotor speed is 0r/min and 6000r/min, respectively. In the case of wave inclination angle from 0 to 18 degrees, when the gyro rotor speed is 0r/min, the ship transverse rocking angle is 0~16 degrees, and in the case of gyro rotor speed is 6000r/min, it is 0~3.5 degrees, and the rocking reduction ability of the rocking reduction double gyro reaches 78.1%.

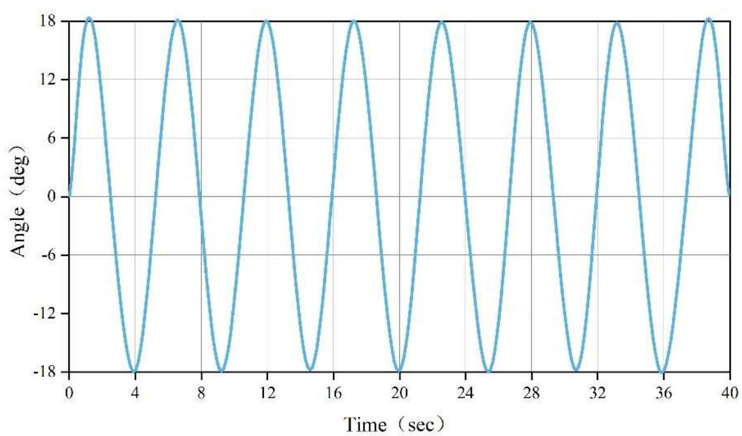


(a) Wave slope

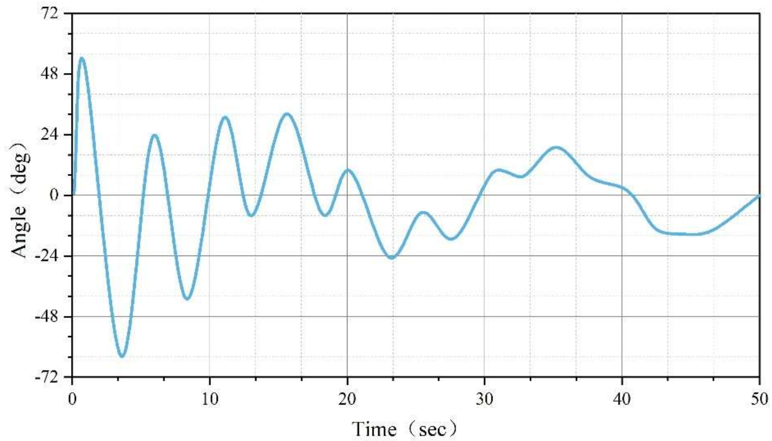


(b) The simulation results of 0r/min

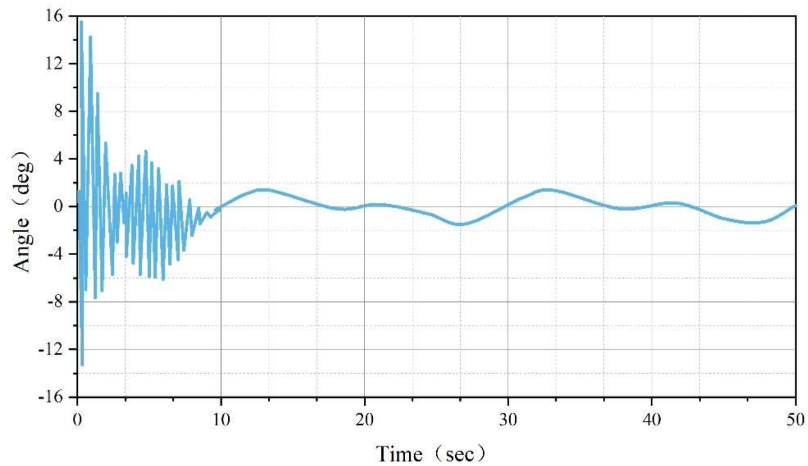


(c) The simulation results of 6000r/min

**Fig. 2.** The simulation results of second-order waves

### *4.3. Tertiary wave reduction performance analysis*

The simulation results obtained by selecting the middle value of the fetch wave height of 0.82 m under the three-level meaningful wave sea state condition are shown in Fig. 3, and Figs. (a)~(c) show the wave inclination angle of the ship, and the transverse rocking angle of the ship at the speed of the dual gyro rotor of 0 r/min and 6000 r/min, respectively. The propagated wave inclination angle is significantly elevated at 0 to 48 degrees in the third level wave environment. When the gyro rotor speed is 0r/min, the ship transverse rocking angle remains at 0~45 degrees, while when the gyro rotor is running and reaches the speed of 6000r/min, the ship transverse rocking angle is approximated to be 0~10 degrees, and the rocking reduction capability reaches 77.78%.

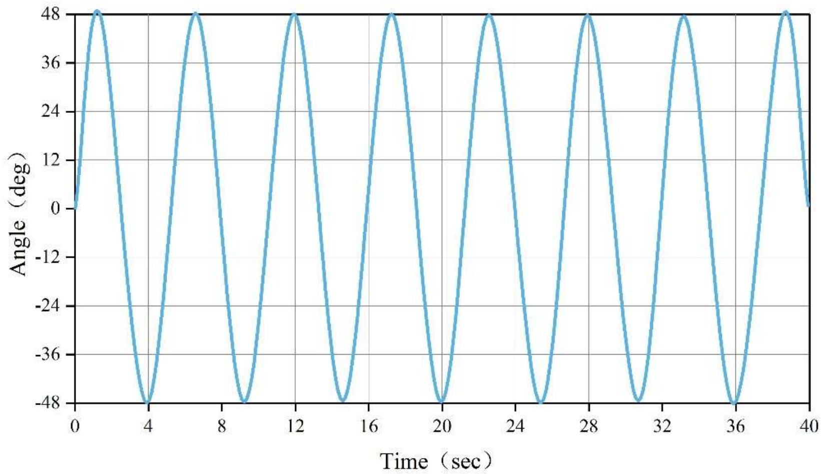


(a)Wave slope

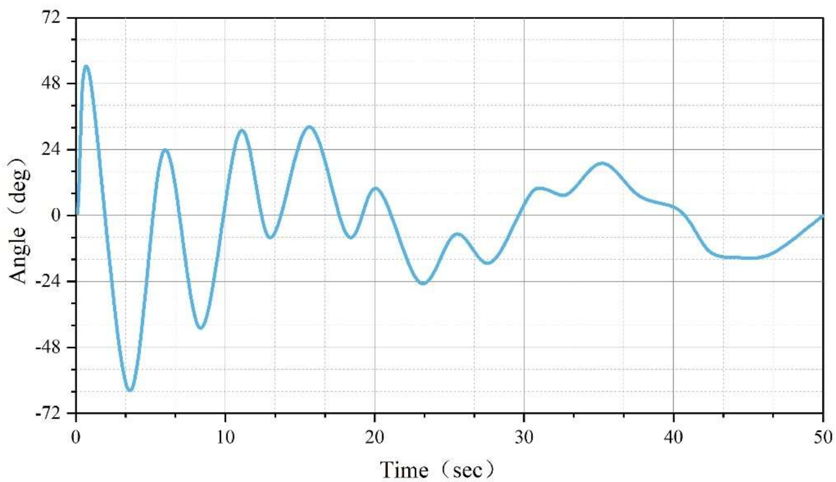


(b)The simulation results of 0r/min

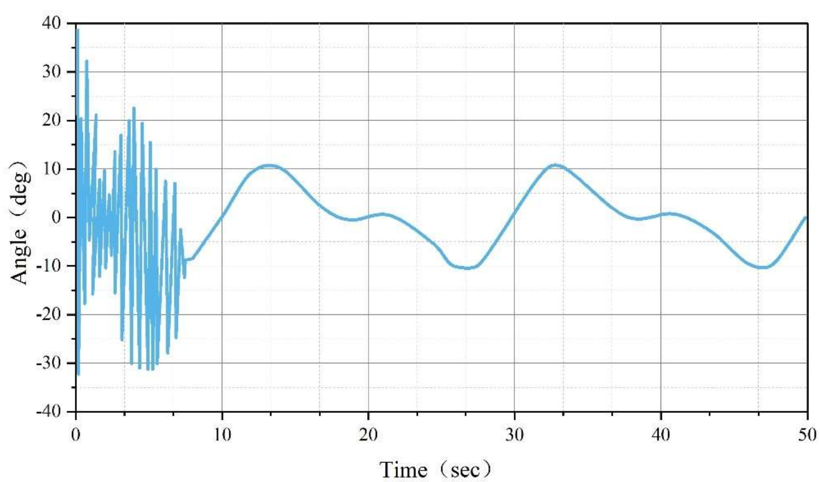


(c))The simulation results of 6000r/min

**Fig. 3.** The simulation results of third-order waves

## *4.4. Analysis of the performance of wave attenuation for class IV waves*

The simulation experiments are carried out under four-level waves with the middle value of wave height of 1.9 meters, and the simulation results obtained are shown in Fig. 4, Figs. (a)~(c) show the ship's wave inclination angle, the ship's transverse rocking angle when the double gyro rotor rotational speeds are 0r/min and 6000r/min, respectively. At this time, the wave inclination angle is at 0~60 degrees. When the dual gyro is on, the gyro rotor speed is 0r/min and the ship's transverse rocking angle reaches 0~57 degrees. After starting, the gyro rotor speed is 6000r/min, the ship's transverse rocking angle is approximated to 0 to 30 degrees, and the rocking reduction capacity is 47.37%.

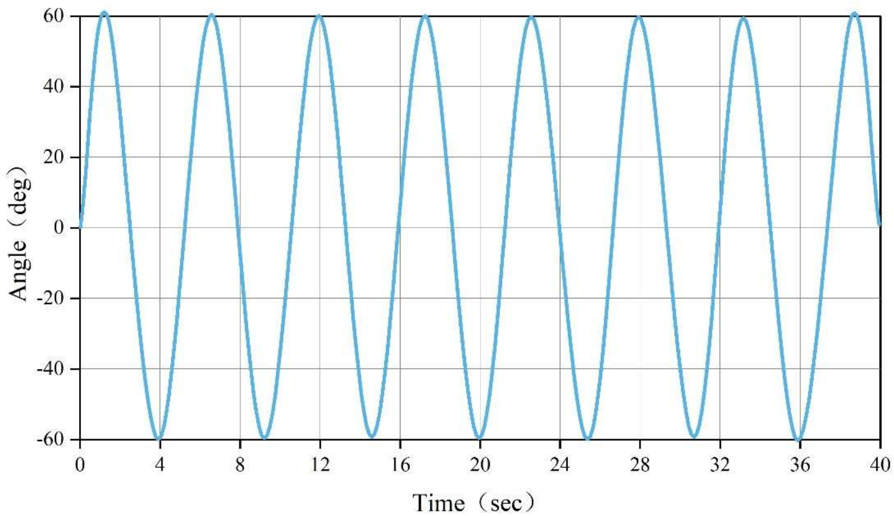


(a)Wave slope

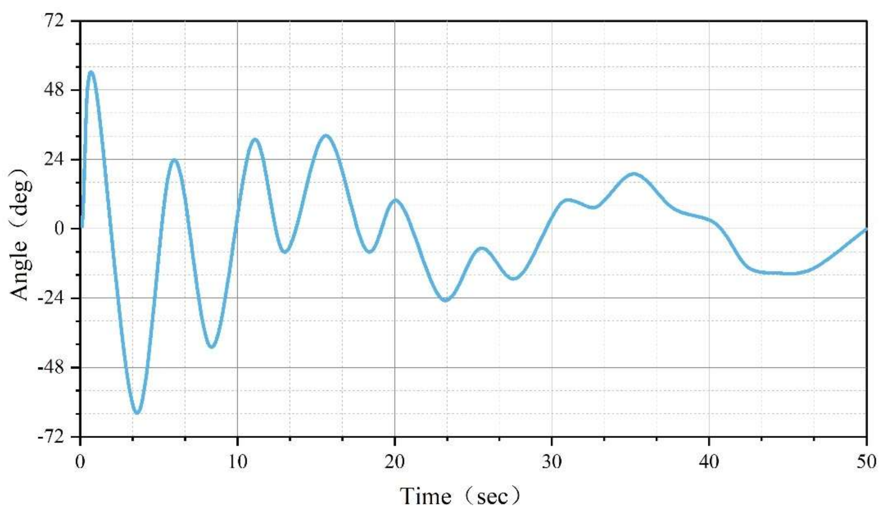


(b)The simulation results of 0r/min

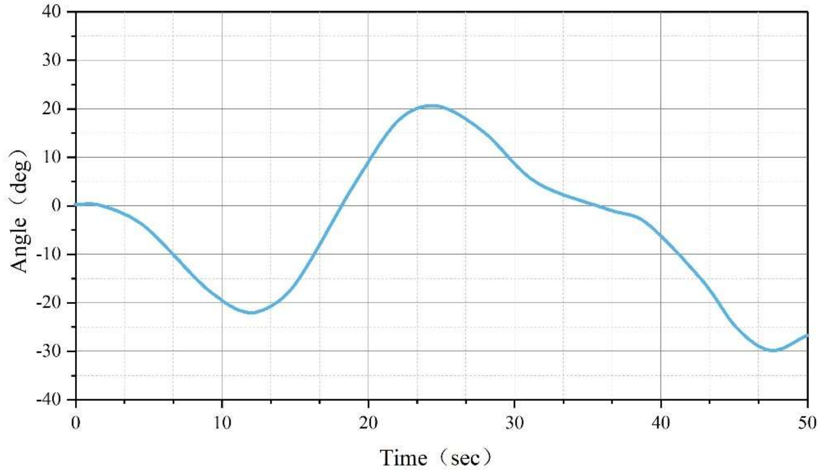


(c))The simulation results of 6000r/min

**Fig. 4.** The simulation results of fourth-order waves

### *4.5. Performance Analysis of Class V Wave Reduction*

The simulation results obtained by taking the middle value of the wave height of 3.2 meters under the sea state of five levels of meaningful waves are shown in Fig. 5, and Figs. (a)~(c) show the wave inclination angle of the ship, and the transverse rocking angle of the ship at the speed of the double gyro rotor of 0r/min and 6000r/min, respectively. From the graphs, it can be concluded that the wave inclination angle is 0~76 degrees at this time. When the gyro rotor speed is 0r/min, the ship transverse rocking angle is 0 to 72 degrees. When the gyro rotor speed is 6000r/min, the rocking reduction double gyro can not play the role of rocking reduction, the ship has the danger of capsizing.

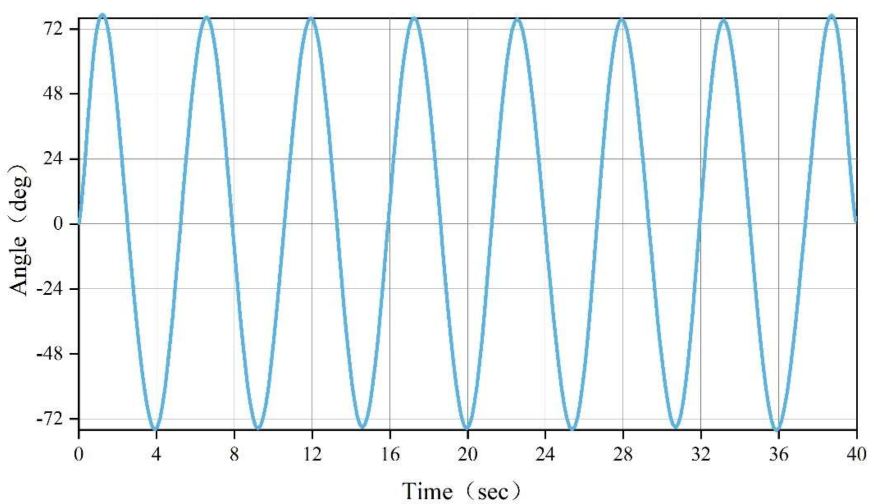


(a)Wave slope

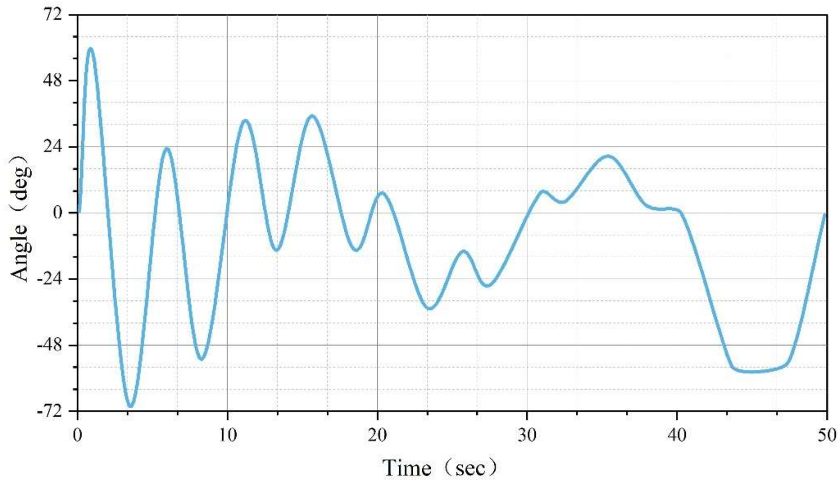


(b)The simulation results of 0r/min

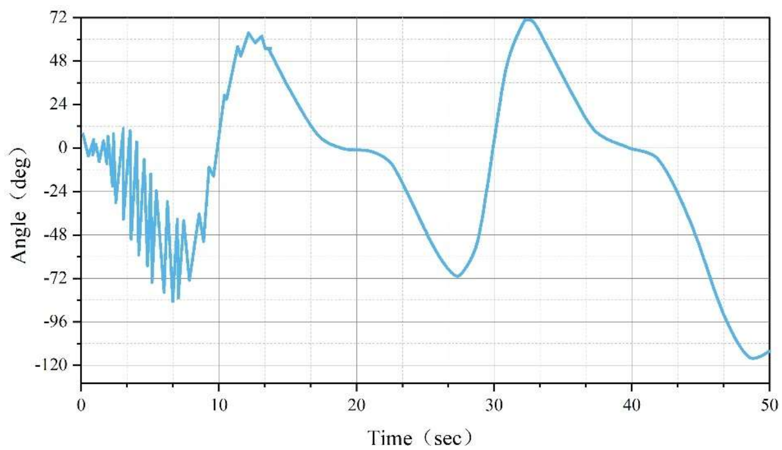


(c))The simulation results of 6000r/min

**Fig. 5.** The simulation results of fifth-order waves

According to the results of simulation experiments, it can be concluded that the double gyroscope designed in this experiment has a very good performance of transverse rocking reduction when the level of meaningful waves is less than or equal to three levels, and even in the first level of waves, the rocking reduction performance can reach more than 80%. When the wave level reaches four, the rocking reduction effect of the dual gyroscope rocking reduction device is greatly weakened. When there is a righteous wave greater than level 5, gyroscopic rocking reduction device can not be effective rocking reduction, the ship is subject to wave shock obviously, but generally to level 4 or level 5 waves, the ship will choose to enter the harbor to avoid the wind. Overall, the double gyro rocking reduction device designed in this paper can have a good rocking reduction performance in complex sea conditions, and further improvement and optimization can be carried out in the future.

## 5. Parameter optimization simulation experiments of a decoupling double gyro

In order to verify the accuracy of the dual gyro parameter optimization model based on multi-objective optimization proposed in this paper, this section will take the unmanned boat "Jinghai" JH-750 of Shanghai University, China, as an example to carry out simulation verification. Firstly, a joint dynamic model is constructed by Matlab/Simulink simulation software, and the transverse rocking angle of the ship when the rocking reduction is off and on is obtained. Then, the parameter optimization model is built to optimize the damping coefficients of the dual gyroscope, and the best damping coefficients are finally obtained.

### *5.1. Simulation and analysis of ship's transverse rocking under complex sea state*

The ocean sea state selected for simulation in this paper is the North Atlantic sea state. According to the statistics of the North Atlantic sea state, this section will carry out the simulation calculation of two kinds of sea state.
1) Sea state 1, with a meaningful wave height of 2.5m and an average period of 7s.
2) Sea state 2, with a meaningful wave height of 2.5m and an average period of 12 s. The simulation time is set to 150s, and the average period is 7s.

The simulation time is set to 150s, and the fixed step size is 0.01s. The simulation results are shown in Table 1. The "off" and "on" in the table represent the maximum transverse rocking angle amplitude when the dual gyro is off and on, respectively. Under sea state 1, the maximum transverse rocking angle decreases from 20.1° to 1.6° after the rocking-reducing gyro is turned on, and the rocking-reducing efficiency is 92.04%. Under sea state 2, the maximum transverse rocking angle amplitude value decreased from 11.3° to 1.2°, and the rocking reduction efficiency was 89.38%. Obviously, after optimizing the parameters of double gyro by using the optimization model of rocking reduction double gyro parameters, the rocking reduction effect of ship's transverse rocking is obvious.

**Table 1.** Simulation results of ship rolling

| Sea state | Closed | Turn on | Anti-rolling efficiency(%) |
|---|---|---|---|
| Sea state 1 | 20.1 | 1.6 | 92.04 |
| Sea state 2 | 11.3 | 1.2 | 89.38 |

### *5.2. Parameter optimization analysis based on bacterial foraging optimization algorithm*

In the parameter optimization model proposed in this paper, the bacterial foraging optimization algorithm is adopted to solve the parameters and realize the parameter optimization of the rocking reduction double gyro. Still taking sea state 1 and sea state 2 proposed above as examples, the results of parameter optimization and rocking reduction performance in different sea states are compared as shown in Table 2. As can be seen from the table, the initial shaking reduction efficiency of the ship's shaking reduction system under the two sea states is 91% and 88.24%, respectively, while the shaking reduction efficiency after parameter optimization is improved by 6.44% and 10.09%, respectively, and the difference in the high-frequency envelope area is relatively small, which indicates that the optimized parameter of the inlet system does not have vibration shaking phenomenon. According to the above results, it proves the effectiveness of the shaking reduction dual gyro parameter optimization model proposed in this paper on the optimization of dual gyro parameters and the positive effect of parameter optimization on the shaking reduction efficiency.

**Table 2.** Parameter optimization results in different sea conditions

| Parameter classification | Parameter name | Optimal results | |
|---|---|---|---|
| | | Sea state 1 | Sea state 2 |
| Initial parameters | Fitness | 0.8875 | 1.022 |
| | Anti-rolling efficiency | 91% | 88.24% |
| | High frequency band envelope area | 3644.22 | 178.74 |
| Optimize parameters | Fitness | 4.8228 | 4.932 |
| | Anti-rolling efficiency | 97.56% | 98.33% |
| | High frequency band envelope area | 3738.85 | 398.34 |

### *5.3. Parameter optimization results and analysis*

In order to further analyze the relationship between parameter optimization and rocking reduction efficiency, this section takes sea state 2 as an example, and analyzes the ship's transverse rocking condition and gyro advancement and output moment before and after parameter optimization, as shown in Fig. 6. Figures (a)~(b) show the optimization results of the ship's transverse rocking angle parameter, the optimization results of the gyro feed angular velocity and the optimization results of the gyro output moment. The dashed, dotted and solid lines in Fig. (a) show the ship's transverse rocking angle when the rocking reduction is turned off, under the initial rocking reduction parameter, and under the optimized rocking reduction parameter, respectively. The maximum transverse rocking amplitude of the ship is 16.1° and the transverse rocking angle trinity is 9.2° under the sea state II environment. Under the initial rocking reduction parameters, the maximum transverse rocking amplitude of the ship is 1.9°, the transverse rocking angle trinity value is 1.1°, and the rocking reduction efficiency is 88.31%. After the parameter optimization, the ship's transverse rocking angle is significantly reduced, with the maximum value of 0.6°, the trinity value of 0.3°, and the rocking reduction efficiency is 97.44%, which is 9.13% higher than that of the initial rocking reduction parameters. As can be seen from Figs. (b) and (c), the control system optimized by the algorithm can output a larger angular velocity and rocking reduction moment, and the optimized rocking reduction gyro output moment is closer to the wave disturbance moment waveform, and there is no jittering phenomenon. When the output moment of the rocking reduction gyro is in the opposite direction to the wave disturbance moment and the size is close to the wave disturbance moment, the rocking reduction effect is better, that is to say, the rocking reduction effect of the ship after parameter optimization is very good.

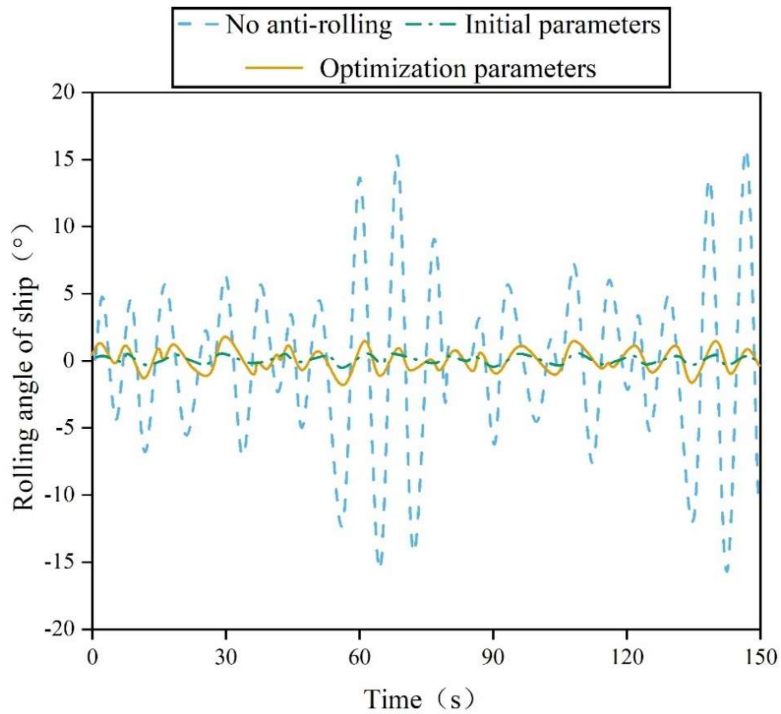


(a)Optimization results of ship roll angle parameters

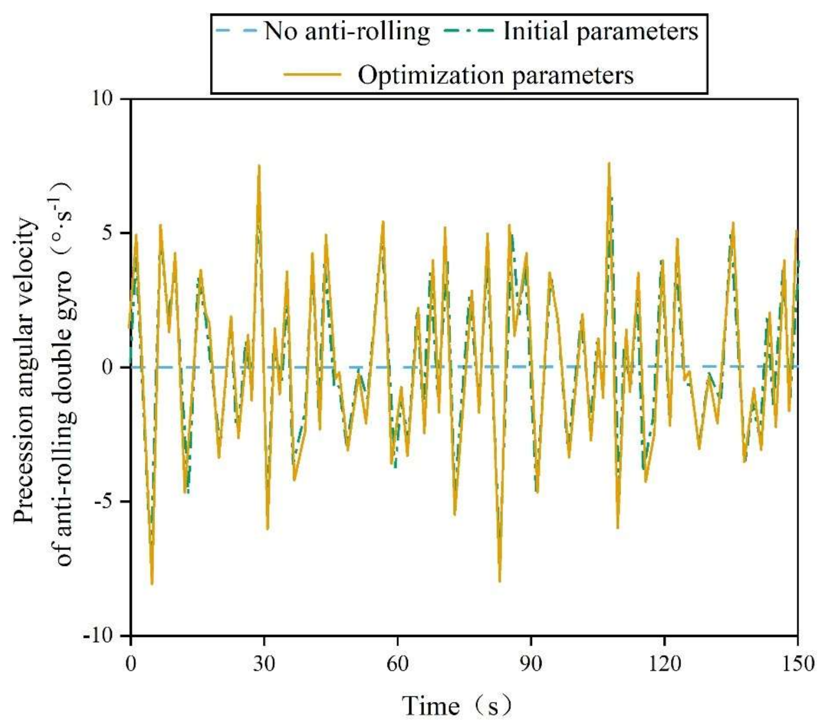


(b)Optimization results of the precession angular velocity of the anti-rolling gyro

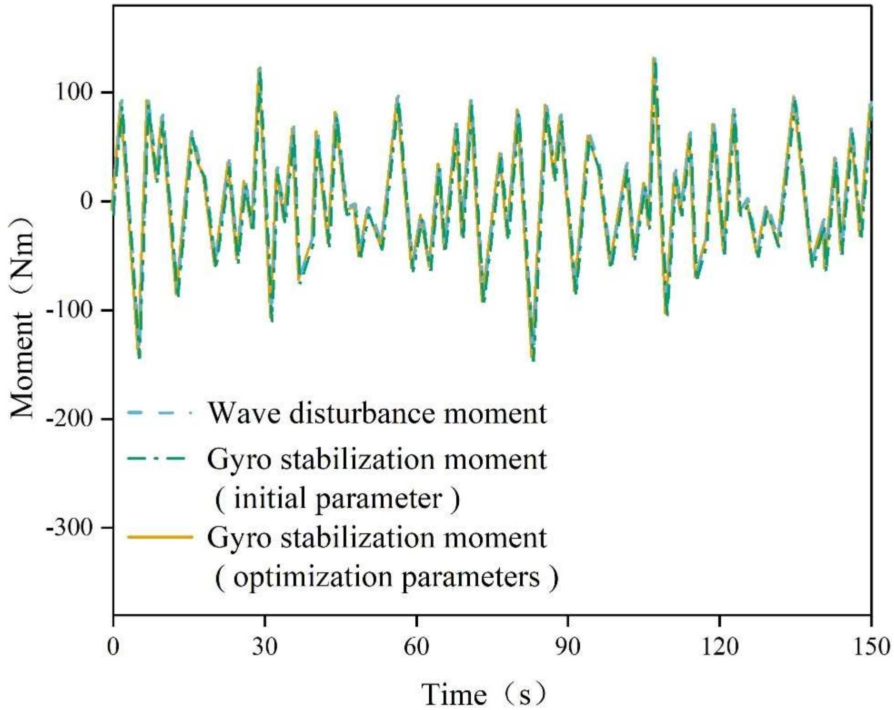


(c)Optimization results of output torque of anti-rolling gyroscope

**Fig. 6.** Optimization results

## 6. Conclusion

The purpose of this paper is to study the rocking reduction performance and law of the double gyro rocking reduction device, to optimize its design, to improve the working performance of the ship-carried rocking reduction double gyro, and to provide assistance for the stable operation of the ship under complex sea conditions. The nonlinear dynamic equations of the double gyro rocking reduction device are established, and its corresponding dynamic model is proposed. Establish the parameter optimization model of the sway-reducing double gyro and propose the parameter optimization method to improve the sway-reducing effect of the sway-reducing double gyro.

Adams is used to carry out dynamic simulation experiments on the rocking reduction double gyro device model proposed in this paper to explore the rocking reduction performance of the rocking reduction double gyro device under different wave levels. In one to three wave levels, when the rotor speed of the double gyro is 0r/min, the wave inclination angle is within 0~4 degrees, 0~16 degrees and 0~48 degrees, respectively, and when the rotor speed is 6000r/min, the maximum transverse rocking angle of the ship is 0~0.4 degrees, 0~3.5 degrees, 0~11 degrees, and the rocking reduction capacity reaches 87.5%, 78.1%, and 77.78%, respectively. Obviously, when the wave level is one to three, this paper's rocking reduction double gyro device shows excellent ship rocking reduction effect. When the wave level reaches four, the rocking reduction capability decreases to 47.37%, and when the wave level reaches five, the rocking reduction effect is no longer available. However, when the wave level is four to five, the ship will basically choose to enter the harbor to avoid the wind, so the proposed rocking reduction dual gyro device model can basically satisfy the daily operation of the ship in complex sea conditions.

Taking “Jinghai” JH-750 unmanned boat of Shanghai University of China as an example, the validity of the optimization method of the rocking reduction double gyro parameters proposed in this paper is examined, and simulation experiments of the optimization of the rocking reduction double gyro parameters are carried out. In the North Atlantic simulation sea state environment of sea state 1 (Yi wave height 2.5m, average period 7s) and sea state 2 (Yi wave height 2.5m, average period 12 s), the rocking reduction efficiency of the rocking reduction double gyro can reach 92.04% and 89.38% respectively, and the maximal transverse rocking angle amplitude value is also decreased from 20.1° and 11.3° to 1.6° and 1.2° respectively, so that the effect of the reduction of the rocking of the ship's transverse rocking is The effect of reducing the ship's transverse rocking is obvious. After adopting the parameter optimization method in this paper, the initial rocking reduction effect of the ship rocking reduction system under sea state 1 and sea state 2 is 91% and 88.24% respectively, which is 6.44% and 10.09% higher than that before optimization.

Overall, the rocking reduction double gyro model based on nonlinear dynamic equations and the rocking reduction double gyro parameter optimization model proposed in this paper can better realize the optimization and improvement of the rocking reduction double gyro, and better enhance its rocking reduction effect on the ship.

## References

[1] Ramirez-Lopez, A. (2024). The Use of Computational Algorithms to Display the Aircraft Instruments That Work with Gyroscopic and Magnetic Physics (Theory for Programming an Elementary Flight Simulator). Applied Sciences, 14(16), 7099.

[2] Cinal, Ş., & Eminoğlu, İ. (2022). MECHANICAL GYROSCOPE-BASED ROLL MOTION REDUCTION OF MARINE VEHICLES: AN EDUCATIONAL SETUP. Journal of Naval Sciences and Engineering, 18(2), 179-204.

[3] Stefanski, K. (2019, February). The analysis of the anti-aircraft missile flight controlled with gyroscopic system. In AIP Conference Proceedings (Vol. 2077, No. 1). AIP Publishing.

[4] Nazemipour, A., Manzuri, M. T., Kamran, D., & Karimian, M. (2020). MEMS gyro bias estimation in accelerated motions using sensor fusion of camera and angular-rate gyroscope. IEEE Transactions on Vehicular Technology, 69(4), 3841-3851.

[5] Saeed, S., Niehoff, J. H., Boriesosdick, J., Michael, A., Schönbeck, D., Wöltjen, M. M., ... & Kroeger, J. R. (2024). Gyroscope-assisted CT-guided puncture improves accuracy and hit rate compared with free-hand puncture: a phantom study. CardioVascular and Interventional Radiology, 1-9.

[6] Passaro, V. M., Cuccovillo, A., Vaiani, L., De Carlo, M., & Campanella, C. E. (2017). Gyroscope technology and applications: A review in the industrial perspective. Sensors, 17(10), 2284.

[7] Usubamatov, R. (2017). Fundamental principles of gyroscope theory. J. Aeronaut. Aerosp. Eng, 6(2).

[8] Cao, J., Luo, Y., Liu, X., Presas, A., Deng, L., Zhao, W., ... & Wang, Z. (2024). Numerical theory and method on the modal behavior of a pump-turbine rotor system considering gyro-effect and added mass effect. Journal of Energy Storage, 85, 111064.

[9] Li, B., Zhang, X., Wang, J., & Chen, N. (2022). Anti-roll characteristics of marine gyrostabilizer based on adaptive control and hydrodynamic simulation. Journal of Marine Science and Engineering, 10(1), 83.

[10] Taskin, M., & Ahan, A. O. (2024). Input saturated $H_\infty$ optimal control to mitigate DTMB 5415 combatant roll motion using anti roll gyro stabilizer. Ocean Engineering, 305, 117913.

[11] Demir, U. (2020). Use of Anti Rolling Gyro (ARG) Optimization Systems For Planing Boats. Uluslararası Doğu Anadolu Fen Mühendislik ve Tasarım Dergisi, 2(2), 247-261.

[12] Náhlík, T., & Smetanová, D. (2018). Applications of gyroscopic effect in transportation. NAŠE MORE: znanstveni časopis za more i pomorstvo, 65(4 Special issue), 293-296.

[13] Damavandi, M., Shafaghat, R., & Dardel, M. (2021). Selection the optimum dimensions for flywheel of Anti-Rolling Gyro which installation on high speed craft. Journal of Marine Science and Technology, 20(1), 109-124.

[14] Talha, M., Asghar, F., & Kim, S. H. (2017). Design of fuzzy tuned PID controller for anti rolling gyro (ARG) stabilizer in ships. International Journal of Fuzzy Logic and Intelligent Systems, 17(3), 210-220.

[15] Institute of Mechanics Technische Universität Berlin Berlin Germany,Institute of Mechanics Technische Universität Berlin Berlin Germany & Institute for Problems in Mechanical Engineering of the Russian Academy of Sciences St. Petersburg Russia. (2020) .Thence the moment of momentum. ZAMM – Journal of Applied Mathematics and Mechanics / Zeitschrift für Angewandte Mathematik und Mechanik(5),n/a-n/a.

[16] L Rojas,M Molina-Cardenas,E Caballero,C Rojas & A Patiño-Vanegas. (2019). Modeling of dynamic mass coupled system with Runge-Kutta fourth order. IOP Conference Series: Materials Science and Engineering(1),012009 (19pp).

[17] Hu Yanjuan,Pan Leiting,Lv Wenjun & Wang Zhanli. (2024). Optimal selection of cloud manufacturing resources based on bacteria foraging optimization. International Journal of Computer Integrated Manufacturing(1-2),165-182.